Smart Structures and Systems, *Vol. 34, No. 2 (2024) 129-143*
https://doi.org/10.12989/sss.2024.34.2.129

Generation of wind turbine blade surface defect dataset based on StyleGAN3 and PBGMs

W.R. Li [1,2,3a], W.H. Zhao*[1], T.T. Wang [1b] and Y.F. Du [1,2,3c]

[1] *Institution of Earthquake Protection and Disaster Mitigation, Lanzhou University of Technology, Lanzhou 730050, China*
[2] *International Research Base on Seismic Mitigation and Isolation of GANSU Province, Lanzhou University of Technology, Lanzhou 730050, China*
[3] *Disaster Prevention and Mitigation Engineering Research Center of Western Civil Engineering, Lanzhou University of Technology, Lanzhou 730050, China*

(*Received April 16, 2024, Revised September 22, 2024, Accepted September 30, 2024*)

Abstract. In recent years, with the vigorous development of visual algorithms, a large amount of research has been conducted on blade surface defect detection methods represented by deep learning. Detection methods based on deep learning models must rely on a large and rich dataset. However, the geographical location and working environment of wind turbines makes it difficult to effectively capture images of blade surface defects, which inevitably hinders visual detection. In response to the challenge of collecting a dataset for surface defects that are difficult to obtain, a multi-class blade surface defect generation method based on the StyleGAN3 (Style Generative Adversarial Networks 3) deep learning model and PBGMs (Physics-Based Graphics Models) method has been proposed. Firstly, a small number of real blade surface defect datasets are trained using the adversarial neural network of the StyleGAN3 deep learning model to generate a large number of high-resolution blade surface defect images. Secondly, the generated images are processed through Matting and Resize operations to create defect foreground images. The blade background images produced using PBGM technology are randomly fused, resulting in a diverse and high-resolution blade surface defect dataset with multiple types of backgrounds. Finally, experimental validation has proven that the adoption of this method can generate images with defect characteristics and high resolution, achieving a proportion of over 98.5%. Additionally, utilizing the EISeg annotation method significantly reduces the annotation time to just 1/7 of the time required for traditional methods. These generated images and annotated data of blade surface defects provide robust support for the detection of blade surface defects.

Keywords: blade surface defects; computer vision; deep learning; PBGMs; structural health monitoring; StyleGAN3

1. Introduction

With the promotion of carbon neutrality goals, renewable energy, represented by wind energy, is efficiently utilized and increasingly relied upon by the global energy industry. The number of wind turbines has experienced exponential growth in recent years, and the development of wind turbine blades is also trending towards longer and more flexible designs (Hernandez-Estrada *et al*. 2021, Oliveira *et al*. 2018). Wind turbines are typically constructed in challenging environments such as mountainous regions, deserts, and coastal areas, with wind turbine blades positioned at higher altitudes. Wind turbine blades operating in these environments are more susceptible to environmental damage (Guo *et al*. 2021). As an essential component of the wind turbine structure, blades play a crucial role in wind power efficiency. However, due to environmental influences, surface defects can accumulate over time and have an impact on the overall performance and integrity of the operating wind turbine structure. Blade failure has consistently remained the main factor causing the abnormal shutdown of wind turbines, which affects the normal power transmission efficiency. Each blade requires more than ten days for maintenance due to failure (Yang and Sun 2013), which results in significant economic losses during this period. The typical service life of wind turbine blades is approximately 20 years. However, if structural damage and collapse occur due to surface defects of the blades, resulting in safety accidents, the potential consequences outweigh the benefits. Regular detection of wind turbine blade damage during the operational lifespan of wind turbine structures is of utmost importance (Ruiz *et al*. 2018).

Most of the current methods for surface defect detection in wind turbine blades still rely on visual inspection or telescopes, which often incur high labor costs and pose certain risks. Some researchers utilize advanced equipment such as acoustic emission, ultrasound, and thermal imaging to detect surface defects on blades (Beganovic and Söffker 2016, Amenabar *et al*. 2011 and Du *et al*. 2020). However, the high cost of equipment such as acoustic emission and thermal imaging, along with the requirement for users to

*Corresponding author, Ph.D. Student,
E-mail: zhaowh@lut.edu.cn
[a] Ph.D., Professor
[b] Master Student
[c] Ph.D., Professor

ISSN: 1738-1584 (Print), 1738-1991 (Online)

possess specific professional knowledge, has limited their widespread use in the surface defect detection of wind turbine blades. Although most existing civil engineering structural health monitoring uses sensors, using contact sensors for monitoring requires attaching the sensors to or directly embedding them into the blades. This method can cause irreversible damage to the blades, thereby affecting their aerodynamic performance and lifespan. Therefore, there is an urgent need for a low-cost, high-precision, non-contact, and non-destructive detection method for the detection of surface defects on blades.

In recent years, due to the rapid advancements in computer technology, there has been significant growth in methods based on visual detection. The non-destructive and efficient advantages of visual technology have increasingly positioned it as one of the most promising methods for detecting surface damage on wind turbine blades (Sony *et al*. 2019 and Zhou *et al*. 2017). In addition to early scholars using traditional algorithms for crack detection in wind turbine blades (Kaewniam *et al*. 2022 and Sun *et al*. 2022), numerous researchers have employed deep learning models for detecting damage on blade surfaces (Moreno *et al*. 2018, Xu *et al*. 2019, Yu *et al*. 2020, and Sarkar and Gunturi 2021). The method based on deep learning model is fast and efficient, but its detection accuracy depends on the capacity of the dataset. A dataset with diverse defects and a substantial number of scenes is an essential prerequisite for adopting deep learning models for accurate detection.

Numerous researchers have conducted extensive research on surface defects of wind turbine blades using deep learning methods (Yang *et al*. 2021 and Zhu *et al*. 2022). However, due to the lack of publicly available datasets for wind turbine blade defects, the existing datasets are all collected by researchers themselves (Wang *et al*. 2019, Wang and Zhang 2017 and Ozbek *et al*. 2013). The primary challenge still lies in the incomplete dataset and small amount of data, which leads to the inability of surface defect detection capability to meet actual detection requirements. Although some scholars have proposed a model-based data augmentation method to expand the dataset of wind turbine structures, this method is not suitable for expanding blade surface defects because it is prone to overfitting during deep learning training (Zhao *et al*. 2023). To tackle the challenge posed by the limited dataset of surface defects on current wind turbine blades, which directly impacts the accuracy of visual detection, it is imperative to develop a method that can substantially augment multi-class defect data.

This paper proposes a data augmentation method based on StyleGAN3 and PBGMs specifically to address the issue of limited data available for wind turbine blade surface defects. This approach solves the problems of low training accuracy and unsatisfactory detection results that arise from the lack of datasets for deep learning models. The specific sections of this paper are as follows: In Section 1, a comprehensive elaboration is provided on the existing surface defect detection methods and the significance of defect datasets. In Section 2, a blade defect dataset expansion framework is constructed by using the StyleGAN3 (Style Generative Adversarial Network 3) deep learning model to generate a blade defect dataset. The foreground defects generated by StyleGAN3 are combined with background images based on physical expansion for blade surface defect fusion. In Section 3, experimental verification was conducted to expand the defect data by comparing it with other GAN models. In Section 4, the method proposed in this paper is used to expand the actual defect dataset, and the EISeg annotation method is combined to accurately annotate the data, ultimately laying the foundation for blade surface defect detection. In Section 5, the main conclusions of this work are summarized.

2. Defect data generation method based on StyleGAN3 deep learning model

The effectiveness of training deep learning models is inherently constrained by the richness of the dataset available. Conventional methods for dataset expansion frequently rely on basic techniques like translation, scaling, and cropping. However, these physical expansion methods often lead to a significant proliferation of duplicate images, consequently increasing the risk of overfitting during the training process. In response to the challenges in dataset collection, this paper proposes a data generation method based on the StyleGAN3 deep learning model to address the issue of difficult data acquisition. Firstly, a small amount of collected real data is combined with the StyleGAN3 deep learning model to generate a large amount of virtual defect data, which is used as the foreground image using image Matting. Secondly, PBGMs are used for blade background construction to achieve rich data types. Finally, fusing the foreground defect image with the background blade image can generate a large and rich defect dataset, as shown in Fig. 1.

2.1 Image generation principle based on GAN deep learning model

Due to the limitations of traditional physical-based image augmentation methods, image generation methods based on Generative Adversarial Networks (GANs) have been gradually proposed and have seen effective development in the era of rapid computer advancement (Goodfellow *et al*. 2014, Arjovsky and Bottou 2017 and Park *et al*. 2017). As shown in Fig. 2, GAN models can proceed through adversarial training using original images that are already available and a noise-input generator. Eventually, the discriminator produces both actual and artificial images, allowing the creation of previously unimaginable images. Multiple fields are currently implementing this method (Park *et al*. 2019, and Chu *et al*. 2020).

With the extensive application of GAN models, numerous scholars have also proposed different types of GAN models. Although GAN-based methods can generate a large number of desired images, the persistent issue remains the inability to generate high-resolution images that closely approach reality. The most crucial aspect of image generation methods based on GAN models is the

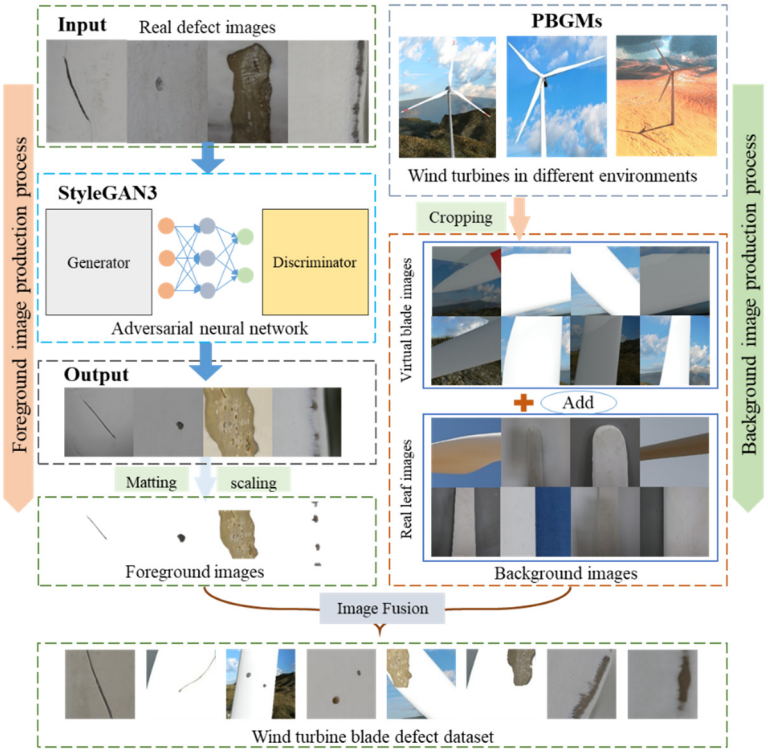

Fig. 1 Production process of wind turbine blade defect dataset based on StyleGAN3 deep learning model

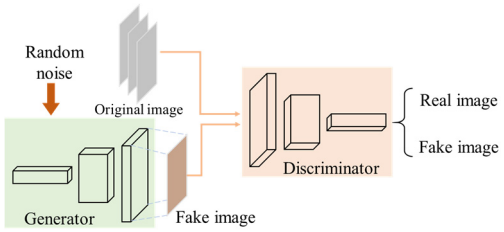

Fig. 2 Image generation principle based on GAN deep learning model

construction of the generator. A well-designed generator can extract the desired image features and control the image synthesis process accordingly. During the sample generation process, the generator may occasionally yield blurry or subpar images, leading to a deficiency in clarity and detail within the generated outcomes. Especially for complex datasets or high-resolution image generation tasks, the problem of pattern blur is more obvious. While striving for diversity in generated outputs by sampling various random noise inputs during the image generation process, this method often introduces significant disorder and randomness, thereby posing a challenge to the precise control of the generated outcomes. Consequently, the generated styles tend to be relatively uniform. GAN models typically demand a substantial volume of training data to attain satisfactory performance, presenting a substantial obstacle when dealing with tasks that involve limited access to, or the acquisition of, extensive annotated data. Therefore, there is a pressing demand for a GAN-based method capable of producing extensive, diverse, and high-resolution images for dataset generation.

2.2 Image generation method based on StyleGAN3 deep learning model

In 2019, the NVIDIA research team proposed the StyleGAN model based on the previous GAN model (Karras *et al.* 2019). This advancement significantly enhanced the quality and diversity of image generation by incorporating Mapping and Synthesis network architectures. StyleGAN introduced the innovative notion of a latent space, characterized by high-dimensional vectors, to exert precise control over the output of the generator. By interpolating in the latent space or modifying different parts of a given vector, control of the generated image can be achieved, such as adjusting expressions, colors, postures, etc. StyleGAN overcomes the problem of pattern collapse in traditional GAN models and exhibits excellent generation ability and diversity. StyleGAN has extensive applications in fields such as facial generation, artistic creation, and virtual games. Due to the presence of artifacts in StyleGAN during image generation, the NVIDIA research team proposed the StyleGAN2 model in 2019 to address this issue (Karras *et al.* 2020). The StyleGAN2 model takes a step further by eliminating initial data processing and eschewing the mean during feature standardization. It incorporates the noise module into the external style module, resulting in superior image generation quality, enhanced feature expression, and more efficient training outcomes.

Despite incorporating layered convolution in StyleGAN2, the conventional synthesis process of adversarial networks still heavily relies on absolute pixel coordinates. This is primarily manifested in the generation of some texture images that adhere to the image coordinates

rather than the intended generation targets. Hence, improvements upon StyleGAN2 led to the introduction of the StyleGAN3 deep learning model (Karras *et al*. 2021), which is the basis for the blade surface dataset in this paper. In the real world, details at different scales are often hierarchical. Current GAN generator architectures utilize low-resolution features for hierarchical refinement by employing up-sampling layers, while introducing novel details through convolutional local mixing and nonlinearity. However, such methods can only have surface similarity and cannot generate natural images. StyleGAN3 introduces a systematic solution to address the aliasing problem caused by pointwise non-linearity in the continuous domain by assessing its impact and implementing suitable low-pass filtering on the outcomes. Once aliasing is completely mitigated to compel the model to achieve a more natural hierarchical refinement, its operational mode will undergo a dramatic transformation. The internal representation now incorporates a coordinate system that enables the accurate attachment of details to the underlying surface. Therefore, the method proposed in StyleGAN3 is to synthesize a stylized image from shallow to deep, coarse to fine, and features from low to high frequencies, primarily employed in facial synthesis. Wind turbine blade surface defect details are intricate, making it a sensible choice to utilize the synthesized stylized images proposed by StyleGAN3 for data augmentation.

To eliminate the existing aliasing issues, the StyleGAN3 deep learning model strictly adheres to the ideal hierarchical information synthesis method, where each layer is constrained to synthesize a specified frequency. Firstly, two sources of aliasing were identified, namely the blurry grid images generated by non-ideal long sampling filters and the application of ReLU or Swish nonlinear activation functions, which resulted in aliasing. Subsequently, the focus shifts to the exploration of methods for realizing continuous and discrete equivalent transformations, accompanied by a thorough reevaluation of the operators currently employed in the model. This includes convolution, down-sampling, up-sampling, activation functions, and filters. The ideal signal Z and the continuous signal z are correlated through the convolution of the ideal difference filter ϕ_s and the dot multiplication of Dirac comb III_s (Dirac comb function)

$$f(z) = \phi_{s'} * F(III_s \odot z) \tag{1}$$

$$F(Z) = III_{s'} \odot f(\phi_{s'} * Z) \tag{2}$$

Where $\odot$ is the point multiplication, $*$ is the convolution.

The convolution of the difference filter ϕ_s and the Dirac comb III_s formula is represented as follows

$$\phi_s(x) = sin\,c\,(sx_0) \cdot sinc(sx_1) \tag{3}$$

$$sinc(sx) = sin(\pi x)\,/(\pi x) \tag{4}$$

$$Dirac\ \ comb\ III_s(x) = \sum_{X \in \mathbb{Z}^2} \left(x - \left(X + \frac{1}{2}\right)/s\right) \tag{5}$$

Where $x \in [0,1]^2 \text{in} z(x)$; ϕ_s has a band limit with $s/2$ along the horizontal and vertical dimensions, f shall not introduce frequency band content that exceeds the output frequency band limit $s'/2$.

Therefore, it is possible to perform operations specified in one domain correspondingly in another domain. After establishing a relationship between the band-limited continuous feature map $z(x)$ and the discretely sampled feature map $Z(x)$, the focus can be shifted away from the pixel center of the signal.

For convolution operations, the StyleGAN3 deep learning model uses standard convolution with discrete convolution kernels K, which are in the same sampling grid with an equal rate of s as the input feature map. Operations in the discrete domain closely resemble convolutional kernels and feature maps, conducting convolution computations along with corresponding window sliding. Since convolution is performed by continuously sliding discrete kernels on the feature map, it can meet the band-limited requirements of translation and rotation. The convolution operation formulas are shown in Eqs. (6)-(7).

$$\begin{aligned} f_{\text{conv}}(z) &= \phi_s * (K * (III_s \odot z)) \\ &= K * (\phi_s * (III_s \odot z)) = K * z \end{aligned} \tag{6}$$

$$\phi_s * (III_s \odot z) = z \tag{7}$$

Ideal up-sampling does not modify the representation of the continuous domain but adds a margin in the spectrum to increase the feasible region. In down-sampling, it is necessary to use low-pass filtering ψ_s on the feature map z to remove frequencies higher than the output frequency band limit, to accurately represent the signal in coarser discretization. The continuous and discrete up-sampling and down-sampling equations for the StyleGAN3 deep learning model are as follows

$$f_{\text{up}}(z) = z \tag{8}$$

$$F_{\text{up}}(Z) = III_{s'} \odot (\phi_s * Z) s' = ns \tag{9}$$

$$f_{\text{downm}}(z) = \psi_{s'} * z \tag{10}$$

$$\psi_{s'} = s^2 \cdot \phi_s \tag{11}$$

$$\begin{aligned} F_{\text{down}}(Z) &= III_{s'} \odot \left(\psi_{s'} * (\phi_s * Z)\right) \\ &= \frac{1}{s^2} \cdot III_{s'} \odot (\psi_{s'} * \psi_s * Z) \\ &= \left(\frac{s}{s}\right)^2 III_{s'} \odot (\phi_s * Z) \end{aligned} \tag{12}$$

Applying an activation function in the continuous domain may introduce high-frequency information. To eliminate potential interference caused by this, convolution with a low-pass filter ψ_s is applied first to remove the high-frequency content. The activation function introduces new frequencies and requires the use of reconstruction filters that conform to the Dirac comb III_s sampling

frequency to limit the range of these frequencies before the final discretization operation. Reconstruction filters for continuous and discrete domains are shown in Eqs. (13)-(14).

$$f_\sigma(z) = \psi_s * \sigma(z) = s^2 \cdot \phi_s * \sigma(z) \tag{13}$$

$$F_\sigma(Z) = s^2 III_{s'} \odot (\phi_s * \sigma(\phi_s * Z) \tag{14}$$

Equivariant operation implies that as the input shifts, the output shifts correspondingly. Regardless of how the input signal rotates in the time domain, each layer of the network adjusts its output accordingly, ultimately resolving the issue of texture alignment.

The generator architecture of the StyleGAN3 model is shown in Fig. 3, and the overall network improvement configuration is described in Table 1.

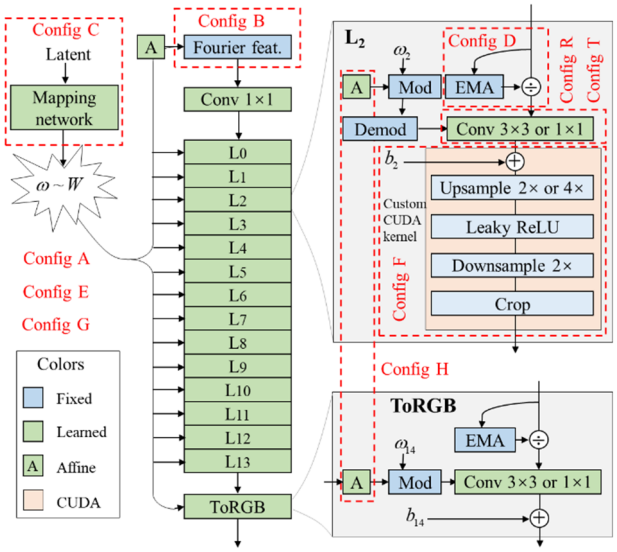

Fig. 3 StyleGAN3 deep learning model generator architecture

From Fig. 3 and Table 1, it can be seen that the StyleGAN3 deep learning model initially employs Fourier features and simplifies the baseline model, removing noise inputs at each layer. The positional information of features is entirely inferred from the coarse features of the preceding layer. Secondly, StyleGAN3 optimized the boundary and up-sampling problems, replacing bilinear sampling with an ideal low-pass filter. Then, nonlinear filtering improvements were made to accelerate the training speed by activating the Leaky ReLU function. Finally, image aliasing is suppressed through translation invariance and rotation invariance. It is noteworthy that utilizing CUDA for network training in Config F accelerates the training speed by nearly 10 times and conserves memory. In summary, the continuous optimization employed by the StyleGAN3 model allows for the generation of a diverse range of styles, high-resolution images, and a large quantity of novel, previously unseen images, making it highly suitable for dataset generation in deep learning applications.

2.3 Generation of foreground defect data based on StyleGAN3

For the generation of defect datasets in the StyleGAN3 deep learning model, it is imperative to have a stable discriminator in place, as demonstrated in Table 2 for the implementation of visual image data generation. In this paper, both real and fake images are generated using multiple convolutional operations, with both the generator and discriminator being utilized for the creation of blade defect data.

The StyleGAN3 deep learning model can generate defect images in multiple styles, but it often virtualizes the background. In practical defect detection scenarios, there may be a variety of backgrounds to contend with. relying solely on a dataset consisting of images with defect data is insufficient to fulfill the requirements of defect detection tasks.

Table 1 StyleGAN3 deep learning model overall network improvement configuration

Configuration	Add module	Improvement
Config A	StyleGAN2	Consistent with StyleGAN2
Config B	Fourier features	Promote precise and continuous translation and rotation transformations of input features
Config C	No noise inputs	Delete noise inputs at each scale to reduce the depth of the mapping network
Config D	Simplified generator	Track all pixels and EMA (Exponential Moving Average) on feature maps during training to eliminate skip connections
Config E	Boundaries and up-sampling	Improve EQ-T (Equalizer T) metrics and reduce FID (Frechet Inception Distance)
Config F	Filtered nonlinearities	Use the Leaky ReLU activation function to accelerate training speed
Config G	Non-critical sampling	Suppress image aliasing, improve translation and other deformations, and reduce FID again
Config H	Transformed fourier features	Output global translation and rotation parameters
Config T	Flexible layers (StyleGAN3-T)	Low-resolution layers attenuate, while high-resolution layers retain high-frequency information
Config R	Rotation equiv. (StyleGAN3-R)	Twice the number of feature mapping layers to compensate for the reduced parameters

Table 2 StyleGAN3 discriminator network structure

Name	Buffers	Output shape
Fromrgb	16	8×512×512
Skip	16	16×256×256
Conv0	16	8×512×512
Conv1	16	16×256×256
Skip	16	32×128×128
Conv0	16	16×256×256
Conv1	16	32×128×128
Skip	16	64×64×64
Conv0	16	32×128×128
Conv1	16	64×64×64
Skip	16	64×32×32
Conv0	16	64×64×64
Conv1	16	64×32×32
Skip	16	64×16×16
Conv0	16	64×32×32
Conv1	16	64×16×16
Skip	16	64×8×8
Conv0	16	64×16×16
Conv1	16	64×8×8
Skip	16	64×4×4
Conv0	16	64×8×8
Conv1	16	64×4×4
Conv	16	64×4×4
FC	16	64

2.4 Fusion of defect data with foreground and background

The background of actual wind turbine blade defect detection is often complex, such as the sky, yellow sand, mountains, etc. The collected images in the field cannot be diversified due to weather, environmental issues, etc. Therefore, this paper combines PBGMs (Physics Based Graphics Models) to generate background images (Narazaki *et al*. 2019 and Hoskere *et al*. 2022). By employing Blender software in conjunction with PBGMs, various environments featuring wind turbine blades are generated to serve as background images. These background images are subsequently merged with defect foreground images generated by the StyleGAN3 deep learning model, culminating in the creation of a high-resolution dataset comprising a substantial number of blade defect images. The process of image fusion is shown in Fig. 4. Firstly, two images to be fused are randomly selected from a large number of foreground and background images, and then the image size is adjusted. To enhance image diversity, this paper aligns the size of the foreground image to match that of the background image. To ensure that all images maintain consistent channels during the fusion process, an Alpha operation is employed to convert the images into a 3-channel format and facilitate weighted fusion. Finally, the fused image is normalized to the range of [0, 255], and the

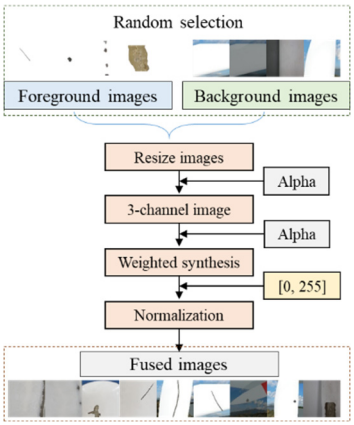

Fig. 4 Steps for the fusion of foreground and background images

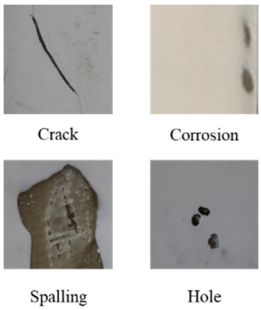

Fig. 5 Real blade defect data images

fused image is ultimately converted into RGB images. This paper randomly combines multiple foreground and background images to generate a substantial quantity of fused images, resulting in the creation of a blade defect dataset.

3. Algorithm verification

3.1 Preliminary data preparation

The prerequisite for utilizing the StyleGAN3 deep learning model for image generation is the requirement of a small number of real images for adversarial training. This paper focuses on four prevalent surface defects found on wind turbine blades, namely Cracks, Corrosions, Spalling, and Holes, as shown in Fig. 5. The authentic images of surface defects on these blades were captured from a small blade model. These surface defects originate from both natural processes that occur over time in the environment, such as corrosions and spalling, as well as artificially induced defects, such as cracks and holes. To enable the StyleGAN3 model to generate effective data in batches, this paper normalizes the previous real defect images, and ultimately all input images have a resolution of 512 × 512.

3.2 Verification of training performance

The hardware used for training the deep learning model in this article consists of an Intel i5 CPU and an NVIDIA

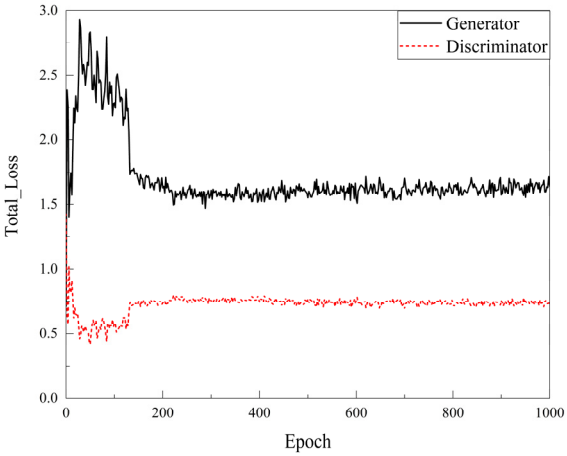

Fig. 6 Comparison of overall loss between generator and discriminator

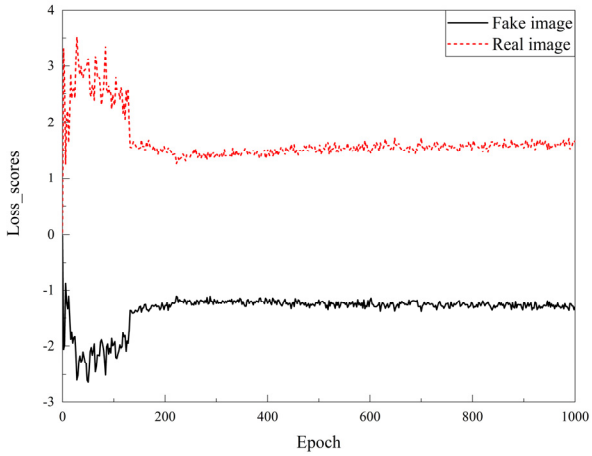

Fig. 7 Comparison of loss functions between real and false images

3060 graphics card with 12 GB of VRAM. The software employed includes Pytorch version 1.11.0, CUDA version 11.3 as the computing resource, complemented by Python version 3.8.2 and Opencv version 4.7.0 for image processing tasks. Due to the limitations of hardware level and unified evaluation of model quality, this paper uses 100 input four types of images for training, and sets batch size = 2, gamma = 6.6, with a unified training setting of 1000 epochs. The StyleGAN3 deep learning model primarily relies on various loss values for its evaluation during the training process. These include the generator and discriminator loss values, the loss values associated with real and fake images, the R1 penalty term loss value, and data augmentation techniques to assess the overall model performance. This paper aims to assess the robustness of the StyleGAN3 deep learning model in generating defect datasets by leveraging three types of loss values.

The StyleGAN3 deep learning model employs a generative adversarial network (GAN) to generate unfamiliar or novel images. Fig. 6 illustrates the cumulative loss of both the generator and discriminator after training for 1000 epochs on crack class defect data. From Fig. 6, it becomes evident that during the training process with the StyleGAN3 deep learning model, the generator and discriminator engage in a simultaneous and dynamic interplay. In the overall training process, the discriminator exhibits relatively stable behavior compared to the generator, and both components tend to reach a more stabilized state after approximately 500 epochs. The data presented in Fig. 6 indicates that the final loss value of the generator stabilizes at 1.63, while the final loss value of the discriminator stabilizes at 0.72. The overall trend of the two is good, and they eventually tend to stabilize. Therefore, the StyleGAN3 deep learning model is capable of generating relatively stable defect images through the interplay between the generator and the discriminator.

In a Generative Adversarial Network (GAN), the primary objective of the generator is to produce realistic images to confound the discriminator to the greatest extent, rendering it incapable of accurately distinguishing between generated images and genuine ones. The generator network is responsible for generating synthesized images, while the discriminator network is responsible for evaluating the differences between the generator output and the real image. Fig. 7 shows the loss functions associated with real and fake images throughout the training process of both the generator and the discriminator.

Throughout the training process, the discriminator endeavors to assign high scores to real images, signifying their likeness to genuine data. The generator minimizes this loss function to improve the quality of the generated image and achieve higher scores in the evaluation of the discriminator. From Fig. 7, it can be observed that the final stabilized loss value for Fake images is -1.31, while the final stabilized loss value for Real images is 1.68. Therefore, the images generated by the StyleGAN3 deep learning model have high quality.

The R1 penalty term is a regularization component utilized to govern the gradient of the discriminator concerning real images. Specifically, the R1 penalty term serves to restrict the magnitude of gradients in the discriminator's assessment of real images. Through gradient regularization, the R1 penalty term contributes to enhancing the stability of GAN training and subsequently elevating the quality of the generated images. Fig. 8 shows the loss value of the R1 penalty term during the training process. The loss value of the R1 penalty term tends to stabilize after 400 epochs. Although the loss value of the R1 penalty term decreased in the last 100 epochs, the overall trend remained stable. Therefore, it indicates that the gradient of the discriminator imposes strong constraints, which helps to stabilize training and improve the quality of generated images.

In the training process of StyleGAN3 deep learning model, it is necessary to introduce data augmentation technology to bolster and improve the robustness of the generator and discriminator, enhance the adaptability of the model to input samples and improve the quality of generated images. The specific approach is to gradually introduce more complex data augmentation strategies. In the early stages of training the StyleGAN3 deep learning model, only simple data augmentation methods such as

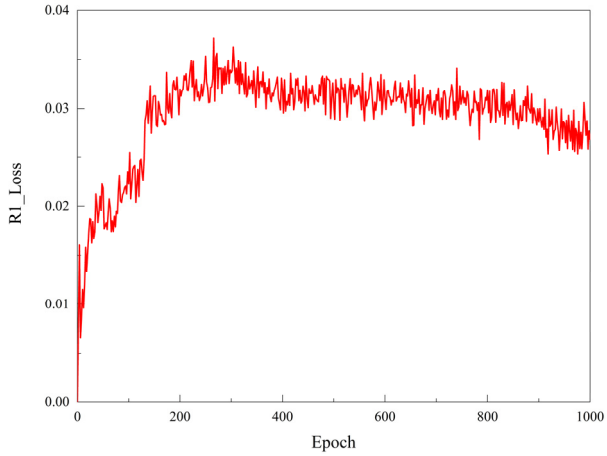

Fig. 8 The loss value of the R1 penalty term

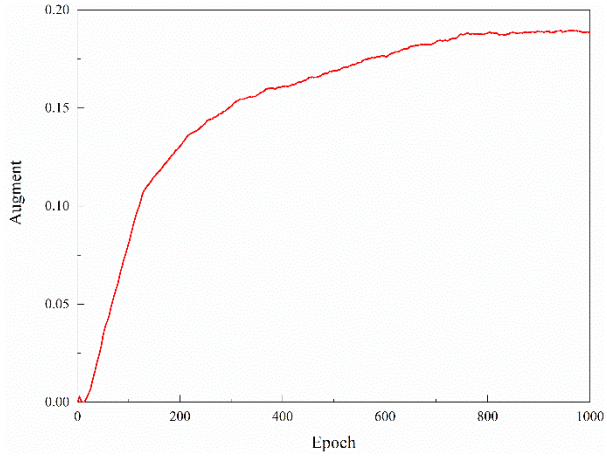

Fig. 9 StyleGAN3 deep learning model data expansion

random translation, rotation, or scaling are used. Then, as the training progresses, more complex enhancement techniques are gradually introduced, such as contrast enhancement, color perturbation, local distortion, etc. Fig. 9 shows the data augmentation process of the StyleGAN3 deep learning model during training. As the number of training iterations increased, the expansion effect consistently improved and eventually stabilized at 1.89 during the last 100 epochs, which is indicative of a favorable expansion effect. The StyleGAN3 deep learning model leverages progressive data augmentation strategies to introduce more advanced enhancement techniques, thereby enhancing the training progress of the model. This iterative approach ultimately leads to an improvement in the quality and diversity of the generated images.

To maintain conciseness in this paper, the training graphs for the remaining three categories of defective data will not be further elaborated upon. The training results for the four categories of defective data images are summarized in Table 3.

From Table 3, it can be seen that the Spalling defect training data is the best among the four types of defect training. All four types of defects exhibit relative stability and demonstrate strong performance. Hence, the training performance of generating blade defect data using the StyleGAN3 deep learning model remains stable and robust. This stability provides valuable support for the generation of defect images.

3.3 Image validation for training

During the training and generation process of adversarial networks, the primary objective of the generator is to produce fake images that closely mimic real ones, aiming to make them indistinguishable from authentic images generated by other models. Through repeated iterative training, the generator continually refines its generation capabilities, leading to the production of fake images that can be on par with real ones in terms of quality. The generated fake image is commonly employed as a means to assess the training effectiveness of the generator, allowing for necessary adjustments and enhancements to the training algorithm. Simultaneously, these synthetic images can also serve the purpose of showcasing the ability of the generator to produce content and assess the effectiveness and quality of the generated output.

To verify the fake images generated through training with the StyleGAN3 deep learning model, this paper conducts comparative experiments using the DCGAN (Deep Convolution Generative Adversarial Networks) deep learning model (Radford *et al.* 2016). The training is performed for 1000 epochs with Crack defects. Extract the input real images separately and train them 1, 100, 300, 800, and 1000 times to generate images. Fig. 10 shows the training results of the DCGAN deep learning model, while Fig. 11 shows the training results of the StyleGAN3 deep learning model. To maintain conciseness in this paper, only 9 images generated during each training are extracted and one image is enlarged for observation.

Fig. 10 reveals that the DCGAN model consistently identifies image features associated with Crack defects throughout the process of generating fake images. The image features progressively become more discernible after 300 epochs. Nevertheless, owing to inherent network depth and structural limitations, even after 1000 epochs, the DCGAN struggles to generate high-resolution fake images

Table 3 StyleGAN3 discriminator network structure

Types of defects	Generator loss	Discriminator loss	Fack image loss	Real image loss	R1 loss	Augment
Crack	1.63	0.72	-1.31	1.68	0.03	0.19
Corrosion	1.57	0.75	-1.23	1.53	0.03	0.34
Spalling	1.61	0.74	-1.25	1.54	0.04	0.40
Hole	1.54	0.70	-1.21	1.82	0.04	0.15

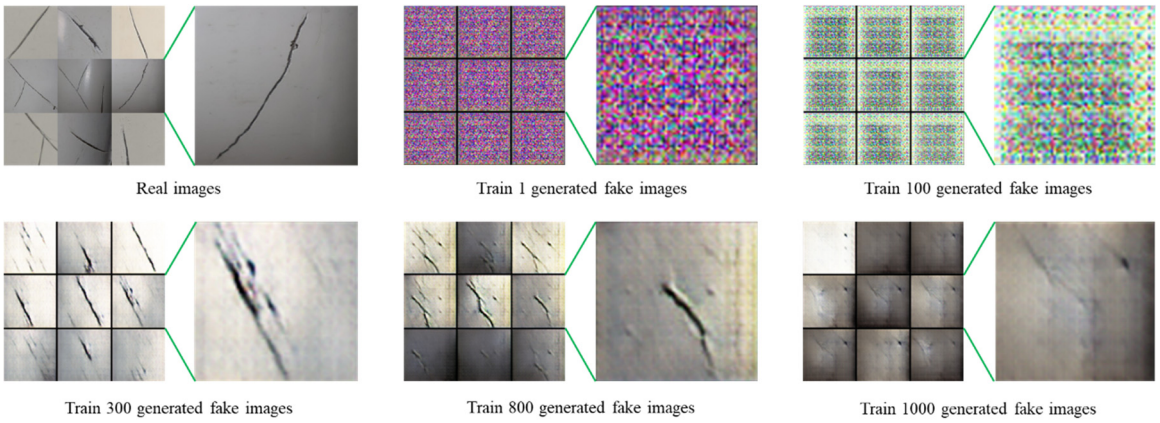

Fig. 10 Training of DCGAN deep learning model to generate fake images

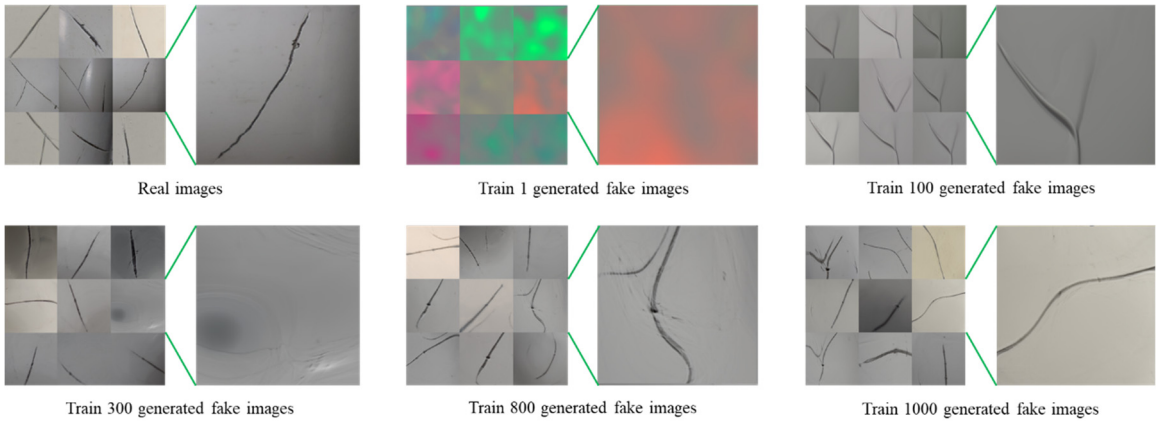

Fig. 11 StyleGAN3 deep learning model training to generate fake images

that can effectively deceive the discriminator. Consequently, DCGAN falls short in generating image data with intricate features like blade defects.

The fake images generated by the StyleGAN3 deep learning model as shown in Fig. 11. Following the initial training epoch, the ability of the model to capture the desired image features is constrained due to its limited learning process. After 100 epochs, the network gradually begins to recognize the features associated with the Crack defect through the adversarial interplay between the generator and discriminator. After 300 epochs, the network becomes capable of producing relatively realistic defect images. However, there are still some fake images that fail to fully extract the evolving features characteristic of Crack images due to incomplete feature capture. Consequently, images without the Crack defect features may appear. After 800 epochs of training, the features of the Crack defect are essentially recognized, and it gradually becomes capable of generating relatively clear images. However, a challenge persists in terms of blending between the background and the generated data, causing localized blurriness in the images. After 1000 epochs of training, the network fully recognizes the features associated with the Crack defect, enabling the generation of entirely clear images. Furthermore, it achieves the ability to distinctly separate the generated data from the background, resulting in the creation of high-resolution images. In the context of blade defect data generation, the StyleGAN3 deep learning model consistently outperforms the DCGAN model in terms of the quality of generated images. Moreover, following 1000 epochs of training, it excels at producing high-resolution fake defect images that are notably clear and prominently showcase distinct defect features. Hence, for subsequent training purposes, it is recommended to consistently employ the StyleGAN3 deep learning model that has been trained for 1000 epochs.

Fig. 12 shows the false images generated by the Coronation, Spalling, and Hole defects of the blades at 1000 epochs. As shown in Fig. 12, it becomes apparent that the fake images resulting from the training of the remaining three types of blade defects closely resemble those of the Crack defect. It gradually acquires defect features after 300 epochs of training, largely obtains defect features after 800 epochs, and fully captures defect features after 1000 epochs, generating high-resolution fake images for the discriminator to discern. Therefore, utilizing the StyleGAN3 deep learning model for the generation of blade defects proves to be a viable approach for augmenting the blade surface defect dataset.

3.4 Image replacement verification

The deep learning model is guided by known input images and target output results to facilitate feature

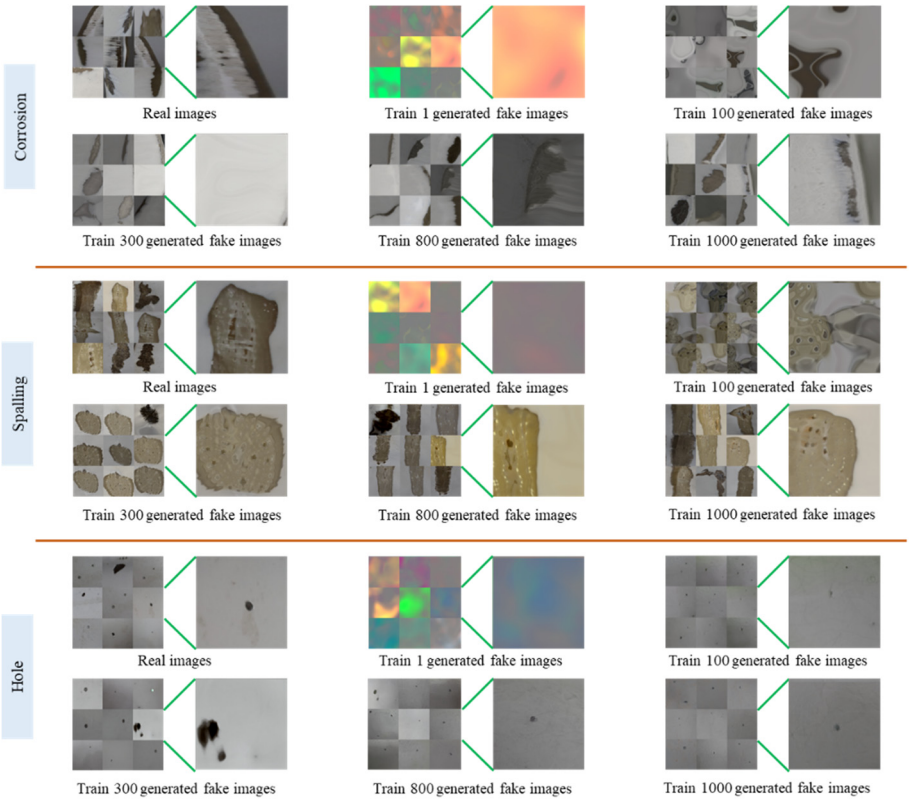

Fig. 12 Generating fake images for the Corrosion, Spalling, and Hole defects on the blades

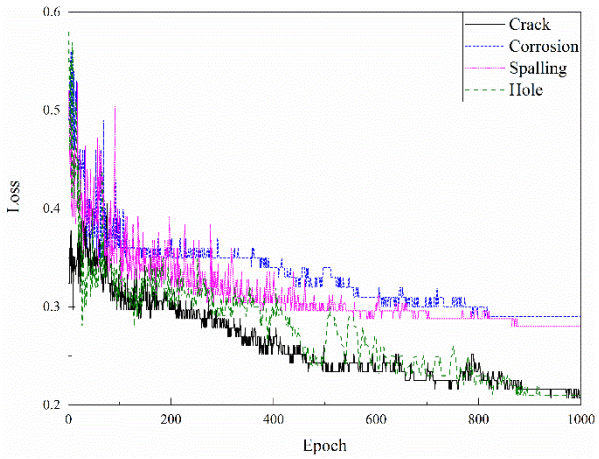

Fig. 13 Replace the loss value of defect images

learning, ultimately deriving the weights for each neural network. These weights are then utilized to formulate rules through shared weight sharing across various layers. The StyleGAN3 deep learning model finds primary applications in the field of facial manipulation and replacement. To validate the results obtained through training with real blade defect data in this paper, a defect replacement approach is employed to verify the effectiveness of the training weights. Untrained blade defect images were used as targets, and defect replacement was executed by leveraging the training weights as connectors to confirm the effectiveness of the training weights outlined in this paper. Fig. 13 shows the loss values of the four types of defects replaced during 1000 iterations, and Fig. 14 shows the corresponding replacement process images.

Figs. 13 and 14 demonstrate that all four types of blade defects can be effectively generated and replaced with non-existent defects by utilizing the trained weights. Fig. 14 reveals that the loss values for cracks and holes decrease at the fastest rate, indicating an effective replacement effect for these defect types. After approximately 300 epochs, the generated images exhibit a high degree of similarity to the target images. Despite the slower decrease in loss values for Corrosion and Spalling images, the generated images still bear a notable resemblance to the target images. Hence, these weights remain suitable for the generation of blade defects. In general, the StyleGAN3 deep learning model demonstrates robust performance in the training of blade defect image generation, making it a viable choice for augmenting the small sample dataset for real blade defect image generation.

4. Dataset generation of blade defects

4.1 Foreground image generation for StyleGAN3 deep learning model

In this paper, a deliberate selection process is undertaken to choose four types of defect images characterized by distinct features and high resolution. Subsequently, the StyleGAN3 deep learning model is employed for image generation. After generating the images, there are still some images that are blurry and have unclear features that cannot be used in the dataset. Table 4

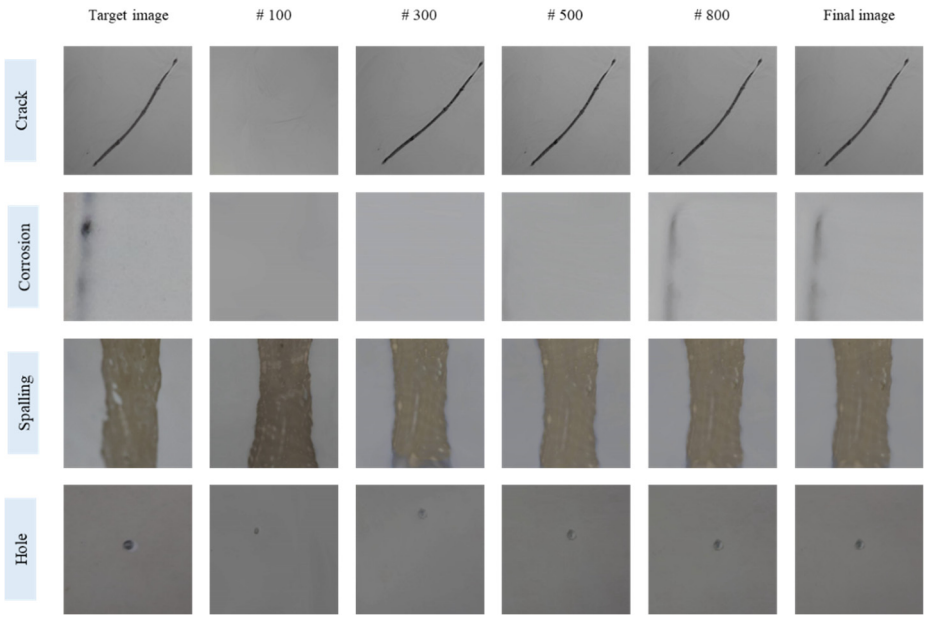

Fig. 14 The process of replacing images with blade defects

Table 4 StyleGAN3 discriminator network structure

Types of defects	Number of original images	Training time	Number of generated images	Number of available images	Percentage of available images
Crack	113	23.08	1000	987	98.7%
Corrosion	133	21.48	1000	923	92.3%
Spalling	88	22.14	1000	978	97.8%
Hole	126	22.02	1000	985	98.5%

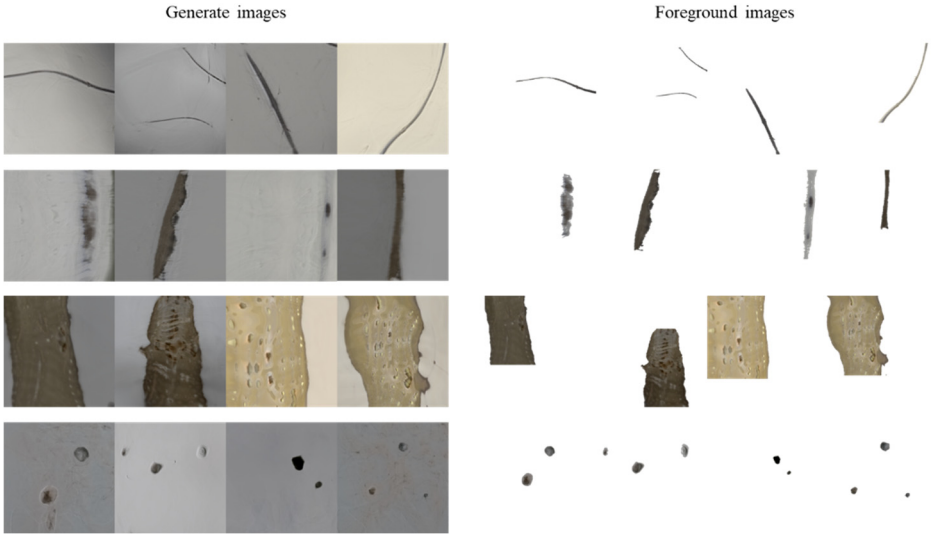

Fig. 15 Defect images and foreground images generated by the StyleGAN3 deep learning model

shows the comparison of the original images, training time, number of generated images, and available images using four types of defects.

The defect images generated by the StyleGAN3 deep learning model showcase robust defect features, albeit occasionally featuring a uniform background. Relying solely on generated defect images for defect training can pose a challenge by overemphasizing positive samples and potentially neglecting the inclusion of negative samples. This could ultimately lead to inefficient defect detection. To enhance the diversity of the dataset, the defect images generated through the StyleGAN3 deep learning model are processed using Matting and Resize operations to create defect foreground images, as shown in Fig. 15. It is worth

noting that the defective foreground images are saved in PNG format, as PNG images support transparent channels, facilitating their fusion with background images.

4.2 Background image creation based on PBGMs and image fusion

To enhance the diversity of the blade defect dataset, this paper employs PBGMs to generate wind turbine models and subsequently extracts cropped blade images to serve as the background images. The PBGM method employed in this paper utilizes Blender software primarily for creating the background of wind turbine blades. Specifically, a wind turbine model is constructed within Blender, and image rendering is performed by setting up different intensities of lighting, various realistic environments, and adjusting the camera positions at different angles. This process ultimately yields high-resolution images of the wind turbine blades. As shown in Fig. 16, various wind turbine models with distinct types, backgrounds, and lighting conditions are generated using the PBGMs method. These models are subsequently locally cropped to generate blade background images. Additionally, real blade images are collected and combined with the PBGMs method to collaboratively create blade background images.

In this paper, the ultimate blade defect dataset is crafted by blending the previously generated blade foreground defect images with the background images. The foreground defect images are in PNG format, while the background images are in JPG format. The foreground image is resized to match the dimensions of the background image, and an Alpha operation is applied to ensure consistency among the image channels. Finally, normalize them into RGB images to form diverse defect data images. It is worth noting that during the fusion process, a random fusion method is employed, which might result in occasional misalignment between the defect position and the blade position. Therefore, it is necessary to remove images with defects that do not match the blade position. Finally, after screening, a total of over 3800 blade defect datasets were generated, with Fig. 17 showcasing a selection of images from the dataset.

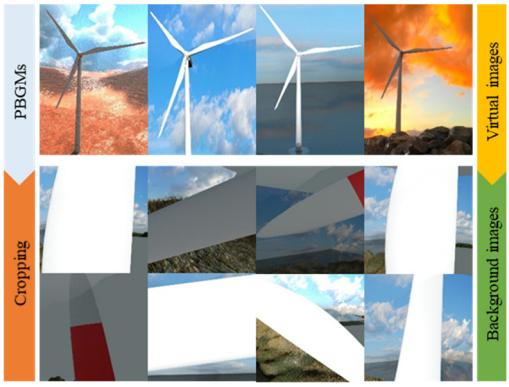

Fig. 16 Creating blade background images using PBGMs

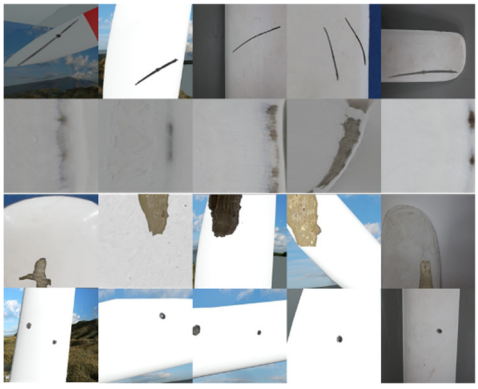

Fig. 17 Some of the created defect images

4.3 Interactive defect data labeling

Accurate visual surface defect detection necessitates precise defect labeling, and the quality of user labeling significantly influences the accuracy of labeling outcomes. Inaccurate labeling can potentially impact the efficacy of subsequent processing and training procedures. Current defect labeling methodologies predominantly depend on tools like LabelMe, which necessitate manual annotation of targets or regions. This manual approach can be resource-intensive and time-consuming, particularly when dealing with extensive datasets. Furthermore, in collaborative labeling scenarios involving multiple individuals, different annotators may adhere to their distinct standards for defect annotation. Consequently, subtle variations in defect color, edge processing, and type differentiation may arise as a consequence of these individual annotator differences. Such discrepancies can potentially introduce confusion between positive and negative samples during the training process, subsequently impacting the accuracy of detection results. Hence, the establishment of a coordinated and standardized defect labeling approach involving multiple individuals holds significant importance.

EISeg (Efficient Interactive Segmentation) is an intelligent and efficient interactive segmentation and labeling software developed using the PaddlePaddle framework (Liu *et al.* 2021). EISeg accomplishes the generation of flexible labeling outcomes by segmenting an image into various target regions, as per the preference of the user for foreground or object areas. This is accomplished by employing a multi-step interactive approach, which offers a semi-automated labeling strategy for image annotation. EISeg provides multiple high-quality interactive segmentation models at different levels for developers to quickly implement semantic and instance label annotation, thereby reducing annotation costs. In contrast to LabelMe, EISeg proves to be better suited for automated image segmentation scenarios, particularly when employing interactive techniques such as threshold adjustments and universal label lists.

Fig. 18 illustrates an example of annotation using EISeg, with Crack defects as an example. When using EISeg for annotation, simply set the segmentation threshold, and then use interactive annotation to set positive and negative sample points for precise annotation. In Fig. 18, the depicted green points denote positive sample points, whereas the red points signify negative sample points.

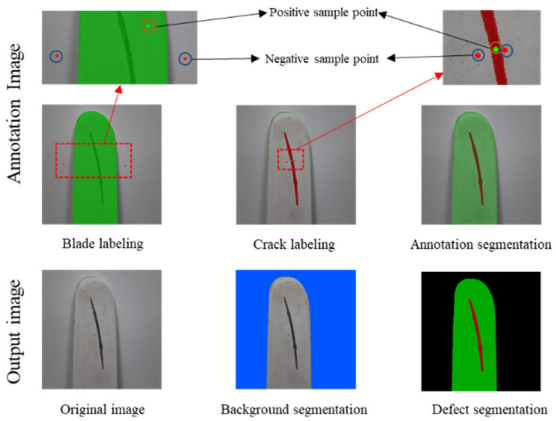

Fig. 18 Example of EISeg annotation

Through the selection of positive and negative sample points, it becomes possible to label the necessary classification samples. EISeg can generate original images, background segmentation images, and defect segmentation images, thereby facilitating a more intuitive examination of annotated segmentation images. It is noteworthy that the time investment for EISeg annotation is merely one-seventh of the time needed for LabelMe annotation. EISeg thus stands out as a tool for efficient and precise annotation.

In this paper, over 3800 blade defect images have been meticulously annotated through the utilization of EISeg. These datasets will serve as a robust foundation for subsequent blade surface defect detection endeavors.

4.4 Defect detection verification

To validate the authenticity of the method proposed in this paper for generating blade defect dataset, two deep learning models, Unet and Deeplabv3+, were employed for verification. Fig. 19 illustrates the outcomes of utilizing the Unet and Deeplabv3+ deep learning models to detect the dataset generated by this paper and real laboratory blade damage images. The training data encompasses Blades, Cracks, Holes, Corrosions, and various mixed defects produced by the method proposed in this paper. From Fig. 19, it is evident that both real and generated defects can be accurately detected by the deep learning models, and different categories of surface defects can also be accurately classified. Therefore, the method proposed in this paper can provide effective support for defect detection based on deep learning models.

5. Conclusions

This paper presents a data augmentation method, which utilizes the StyleGAN3 deep learning model, to tackle the challenge of inadequate datasets concerning wind turbine blade surface defects. Firstly, an expanded framework for the blade defect dataset is constructed, and the StyleGAN3 deep learning model is utilized to generate four types of blade defect images. Secondly, the generated blade defect image is transformed into a defect foreground image through Matting and Resize operations. Then, virtual wind turbine models were generated using PBGMs technology within various environmental contexts, while blade background images were crafted from actual captured images to enhance the diversity of blade surface defects. Subsequently, the foreground and background images generated are randomly blended to create a large, diverse, and high-resolution dataset of blade defect images. Finally, the EISeg annotation method was used for precise data annotation, ultimately laying the foundation for blade surface defect detection. From this research, the following conclusions can be drawn:

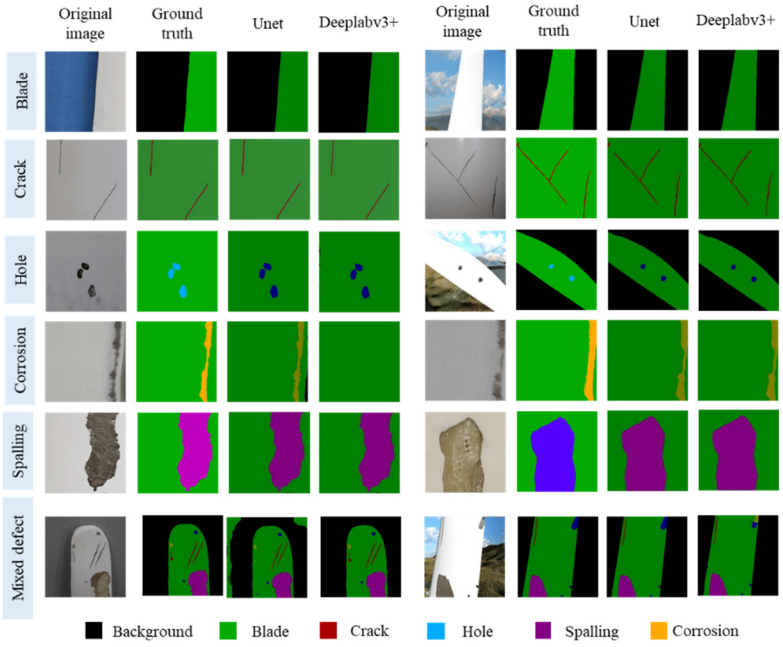

Fig. 19 Example of defect detection algorithm validation

(1) The adversarial generative network based on the StyleGAN3 deep learning model exhibits high performance during training. Both the generator and discriminator losses converge efficiently, enabling the generation of a substantial quantity of diverse, high-resolution blade surface defect images, even when working with a limited sample dataset.
(2) Four common surface defects of the blade were generated based on the StyleGAN3 deep learning model. Among 1000 generated images, the percentage of images that exhibit defect characteristics and maintain high resolution exceeds 98.5%.
(3) The generated defect images are processed into defect foreground images through Matting and Resize operations, while blade background images are generated utilizing PBGMs technology. The foreground and background images are randomly fused. More than 3800 high-resolution images with diverse and multi-class backgrounds were produced. The resulting blade dataset is suitable for training in visual defect detection.
(4) Four common surface defects of the blade were generated based on the StyleGAN3 deep learning model. Using the EISeg annotation method to accurately annotate the surface defect dataset can save 1/7 of the traditional annotation time and provide substantial support for blade surface defect detection.

In order to effectively solve the problem of the lack of surface defect detection dataset for large wind turbine blades, we publicly disclose the defect dataset and corresponding annotated data generated by the method in this paper, and hope that more effective blade surface defect detection methods will be proposed by researchers. This dataset can be found at: https://github.com/zhaowenhai2023/Wind-turbine-blade-surface-defect-dataset.

Acknowledgments

The research described in this paper was financially supported by the National Science Foundation of China (Grant Nos. 52068049 and 51908266), the Science Fund for Distinguished Young Scholars of Gansu Province (No. 21JR7RA267), and Hongliu Outstanding Young Talents Program of Lanzhou University of Technology.

References

Amenabar, I., Mendikute, A., López-Arraiza, A., Lizaranzu, M. and Aurrekoetxea, J. (2011), "Comparison and analysis of non-destructive testing techniques suitable for delamination inspection in wind turbine blades", *Compos. B. Eng.*, **42**(5), 1298-1305. https://doi.org/10.1016/j.compositesb.2011.01.025

Arjovsky, M. and Bottou, L. (2017), "Towards principled methods for training generative adversarial networks", *Proc. ICLR*, 1-17. https://doi.org/10.48550/arXiv.1701.04862

Beganovic, N. and Söffker, D. (2016), "Structural health management utilization for lifetime prognosis and advanced control strategy deployment of wind turbines: An overview and outlook concerning actual methods, tools, and obtained results", *Renew. Sustain. Energy Rev.*, **64**, 68-83. https://doi.org/10.1016/j.rser.2016.05.083

Chu, M., Xie, Y., Mayer, J., Leal-Taixé, L. and Thuerey, N. (2020), "Learning temporal coherence via self-supervision for GAN-based video generation", *ACM Trans. Graph.*, **39**(4), 75:1-75:13. https://doi.org/10.1145/3386569.3392457

Du, Y., Zhou, S., Jing, X., Peng, Y., Wu, H. and Kwok, N. (2020), "Damage detection techniques for wind turbine blades: A review", *Mech. Syst. Signal Process.*, **141**, 106445. https://doi.org/10.1016/j.ymssp.2019.106445

Goodfellow, I., Pouget-Abadie, J., Mirza, M., Xu, B., Warde-Farley, D., Ozair, S., Courville, A. and Bengio, Y. (2014), "Generative adversarial nets", *Proc. NIPS*, **27**, 2672-2680. https://doi.org/10.12989/sss.2023.31.5.469

Guo, J., Liu, C., Cao, J. and Jiang, D. (2021), "Damage identification of wind turbine blades with deep convolutional neural networks", *Renew. Energy*, **174**, 122-133. https://doi.org/10.1016/j.renene.2021.04.040

Hernandez-Estrada, E., Lastres-Danguillecourt, O., Robles-Ocampo, J.B., Lopez-Lopez, A., Sevilla-Camacho, P.Y., Perez-Sariñana, B.Y. and Dorrego-Portela, J.R. (2021), "Considerations for the structural analysis and design of wind turbine towers: A review", *Renew. Sust. Energ. Rev.*, **137**, 110447. https://doi.org/10.1016/j.rser.2020.110447

Hoskere, V., Narazaki, Y. and Spencer Jr, B.F. (2022), "Physics-based graphics models in 3D synthetic environments as autonomous vision-based inspection testbeds", *Sensors*, **22**(2), 532. https://doi.org/10.3390/s22020532

Kaewniam, P., Cao, M., Alkayem, N.F., Li, D. and Manoach, E. (2022), "Recent advances in damage detection of wind turbine blades: A state-of-the-art review", *Renew. Sust. Energ. Rev.*, **167**, 112723. https://doi.org/10.1016/j.rser.2022.112723

Karras, T., Laine, S. and Aila, T. (2019), "A style-based generator architecture for generative adversarial networks", In: *Proceedings of the IEEE/CVF Conference on Computer Vision and Pattern Recognition* (*CVPR*), Long Beach, CA, USA, June.

Karras, T., Laine, S., Aittala, M., Hellsten, J., Lehtinen, J. and Aila, T. (2020), "Analyzing and improving the image quality of stylegan", In: *Proceedings of the IEEE/CVF conference on computer vision and pattern recognition* (*CVPR*), Seattle, WA, USA, June.

Karras, T., Aittala, M., Laine, S., Härkönen E., Hellsten, J., Lehtinen, J. and Aila. T. (2021), "Alias-free generative adversarial networks", *Adv. Neural Inf. Process. Syst.*, **34**, 852-863.

Liu, Y., Chu, L., Chen, G., Wu, Z., Chen, Z., Lai, B. and Hao, Y. (2021), "Paddleseg: A high-efficient development toolkit for image segmentation", arXiv preprint arXiv:2101.06175 [cs.LG]. https://doi.org/10.48550/arXiv.2101.06175

Moreno, S., Peña, M., Toledo, A., Treviño, R. and Ponce, H. (2018), "A new vision-based method using deep learning for damage inspection in wind turbine blades", In: *The 15th International Conference on Electrical Engineering, Computing Science and Automatic Control* (*CCE*), Mexico City, Mexico, September.

Narazaki, Y., Hoskere, V., Eick, B.A., Smith, M.D. and Spencer, B.F. (2019), "Vision-based dense displacement and strain estimation of miter gates with the performance evaluation using physics-based graphics models", *Smart Struct. Syst., Int. J.*, **24**(6), 709-721. https://doi.org/10.12989/sss.2019.24.6.709

Oliveira, G., Magalhães, F., Cunha, Á. and Caetano, E. (2018), "Continuous dynamic monitoring of an onshore wind turbine", *Eng. Struct.*, **164**, 22-39. https://doi.org/10.1016/j.engstruct.2018.02.030

Ozbek, M., Meng, F. and Rixen, D.J. (2013), "Challenges in testing and monitoring the in-operation vibration characteristics of wind turbines", *Mech. Syst. Signal Process*, **41**(1-2), 649-666. https://doi.org/10.1016/j.ymssp.2013.07.023

Park, T., Zhu, J.Y., Wang, O., Lu, J., Shechtman, E., Efros, A.A. and Zhang, R. (2017), "Swapping autoencoder for deep image manipulation", *Adv. Neural. Inf. Process. Syst.*, **33**, 7198-7211.

Park, T., Liu, M.Y., Wang, T.C. and Zhu, J.Y. (2019), "Semantic image synthesis with spatially-adaptive normalization", In: *Proceedings of the IEEE/CVF Conference on Computer Vision and Pattern Recognition* (*CVPR*), Long Beach, CA, USA, June.

Radford, A., Metz, L. and Chintala, S. (2016), "Unsupervised representation learning with deep convolutional generative adversarial networks", arXiv:1511.06434 [cs.LG]. https://doi.org/10.48550/arXiv.1511.06434

Ruiz, M., Mujica, L.E., Alferez, S., Acho, L., Tutivén, L., Vidal, Y., Rodellar, J. and Pozo, F. (2018), "Wind turbine fault detection and classification by means of image texture analysis", *Mech. Syst. Signal Process*, **107**, 149-167. https://doi.org/10.1016/j.ymssp.2017.12.035

Sarkar, D. and Gunturi, S.K. (2021), "Wind turbine blade structural state evaluation by hybrid object detector relying on deep learning models", *J. Amb. Intel. Hum. Comp.*, **12**, 8535-8548. https://doi.org/10.1007/s12652-020-02587-7

Sony, S., Laventure, S. and Sadhu, A. (2019), "A literature review of next-generation smart sensing technology in structural health monitoring", *Struct. Control Health Monit.*, **26**(3), e2321. https://doi.org/10.1002/stc.2321

Sun, S., Wang, T., Yang, H. and Chu, F. (2022), "Damage identification of wind turbine blades using an adaptive method for compressive beamforming based on the generalized minimax-concave penalty function", *Renew. Energy*, **181**, 59-70. https://doi.org/10.1016/j.renene.2021.09.024

Wang, L. and Zhang, Z. (2017), "Automatic detection of wind turbine blade surface cracks based on UAV-taken images", *IEEE Trans. Ind. Electron*, **64**(9), 7293-7303. https://doi.org/10.1109/TIE.2017.2682037

Wang, L., Zhang, Z. and Luo, X. (2019), "A two-stage data-driven approach for image-based wind turbine blade crack inspections", *IEEE ASME Trans. Mechatron*, **24**(3), 1271-1281. https://doi.org/10.1109/TMECH.2019.2908233

Xu, D., Wen, C. and Liu, J. (2019), "Wind turbine blade surface inspection based on deep learning and UAV-taken images", *J. Renew Sustain. Energy*, **11**(5), 053305. https://doi.org/10.1063/1.5113532

Yang, B. and Sun, D. (2013), "Testing, inspecting and monitoring technologies for wind turbine blades: A survey", *Renew. Sustain. Energy Rev.*, **22**, 515-526. https://doi.org/10.1016/j.rser.2012.12.056

Yang, X., Zhang, Y., Lv, W. and Wang, D. (2021), "Image recognition of wind turbine blade damage based on a deep learning model with transfer learning and an ensemble learning classifier", *Renew. Energy*, **163**, 386-397. https://doi.org/10.1016/j.renene.2020.08.125

Yu, Y., Cao, H., Yan, X., Wang, T. and Ge, S.S. (2020), "Defect identification of wind turbine blades based on defect semantic features with transfer feature extractor", *Neurocomputing*, **367**, 1-9. https://doi.org/10.1016/j.neucom.2019.09.071

Zhao, W.H., Li, W.R., Yang, M.H., Hong, Na. and Du, Y.F. (2023), "Dynamic characteristics monitoring of wind turbine blades based on improved YOLOv5 deep learning model", *Smart Struct. Syst., Int. J.*, **31**(5), 469-483. https://doi.org/10.12989/sss.2023.31.5.469

Zhou, H.F., Zheng, J.F., Xie, Z.L., Lu, L.J., Ni, Y.Q. and Ko, J.M. (2017), "Temperature effects on vision measurement system in long-term continuous monitoring of displacement", *Renew. Energy*, **114**, 968-983. https://doi.org/10.1016/j.renene.2017.07.104

Zhu, X., Hang, X., Gao, X., Yang, X., Xu, Z., Wang, Y. and Liu, H. (2022), "Research on crack detection method of wind turbine blade based on a deep learning method", *Appl. Energy*, **328**, 120241. https://doi.org/10.1016/j.apenergy.2022.120241